ACS EARTH AND SPACE CHEMISTRY

http://pubs.acs.org/journal/aesccq

Article

Enhanced Gas Uptake during α-Pinene Ozonolysis Points to a Burying Mechanism

Allison C. Vander Wall, Lisa M. Wingen, Véronique Perraud, Yue Zhao, and Barbara J. Finlayson-Pitts*

Cite This: *ACS Earth Space Chem.* 2020, 4, 1435−1447

Read Online

ACCESS | Metrics & More | Article Recommendations | Supporting Information

ABSTRACT: Understanding how gases interact with and are incorporated into atmospheric secondary organic aerosol particles is crucial for predicting particle effects on climate and human health. This work examined how three gaseous organic nitrates (ON) are taken up into viscous particles formed from the ozonolysis of α-pinene (AP). Experiments were performed in a flow reactor at room temperature under dry conditions, either with or without an OH scavenger present, with constant ozone and variable AP concentrations. Each ON was introduced independently into the flow reactor and was present during particle formation/growth. ON gas-phase concentrations were determined by gas chromatography−mass spectrometry, and particle phase concentrations were measured by high-resolution time-of-flight aerosol mass spectrometry. Partition coefficients (K_{SOA}) for each ON were independent of the initial AP concentration, except for 2-ethylhexyl nitrate which was undetectable in the particles at the lowest AP concentration. Measured K_{SOA} values were larger than those previously determined for equilibrium partitioning, which points to a potential burying mechanism for incorporation of ON during particle growth. Estimated effective net uptake coefficients (γ_{ON}) were found to increase with initial AP concentration. Concentrations of gas-phase oxidation products (including dimers and autoxidation products) predicted using an updated master chemical mechanism increased with AP concentration, with little change in the overall species distribution, consistent with increased trapping/burying of ON during particle growth and thus increased values of γ_{ON}. These results provide further evidence that kinetically controlled burying can contribute significantly to particle growth, provided that the incoming gas-phase molecules have sufficient residence time on the particle surface to become buried *via* subsequent gas−surface collisions.

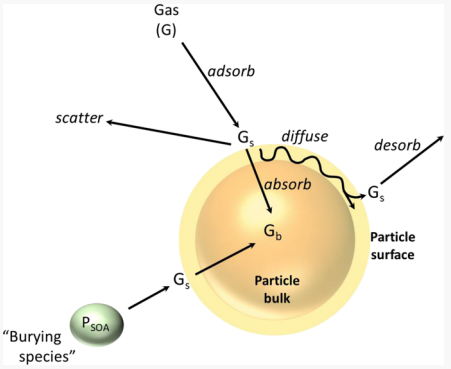

KEYWORDS: *secondary organic aerosol, kinetically limited growth, burying mechanism, α-pinene, ozonolysis, organic nitrate, gas−particle partitioning*

INTRODUCTION

Oxidation of volatile organic compounds (VOCs) in the atmosphere can result in low volatility species that either condense together to form new particles or condense onto and grow existing particles.[1,2] These secondary organic aerosol (SOA) particles play an important role in Earth's radiative budget directly through light scattering and indirectly by acting as cloud condensation nuclei.[3−8] They have also been shown to have deleterious effects on human health.[9−17] Although great progress has been made in understanding how gases are incorporated into particles to contribute to particle growth, these processes are still not completely understood or parameterized by models.[18]

During growth of a liquid droplet, gases diffuse into and out of the particle quickly, establishing a relatively rapid quasi-equilibrium.[19−24] However, many SOA particles have been shown to be more viscous in nature.[25−42] Under high viscosity conditions, diffusion into the particle is slow, and thus, equilibrium timescales can be in the order of minutes to hours because of kinetic limitations.[43−45] Knowledge of particle-phase diffusion coefficients and particle viscosities is therefore required to accurately predict particle composition and growth.[29,46−50] For example, diffusion limited uptake and evaporation of gases can lead to nonuniform particle composition,[51] including the formation of a more semisolid outer "crust" relative to the particle core, which further modifies gas uptake.[30,46,52]

The evidence that under many atmospheric conditions, SOA particles such as those formed from α-pinene (AP) ozonolysis are highly viscous is strong.[25−42] Renbaum-Wolff *et al.*[31] used a poke-flow method to show that SOA particles formed from AP ozonolysis remain highly viscous over a wide range of relative humidities (RH), and particle impaction/bounce experi-

Received: June 19, 2020
Revised: July 17, 2020
Accepted: July 20, 2020
Published: August 7, 2020

ments[34,35] showed that these particles maintained a high rebound fraction up to ~70% RH. Gong *et al.*[53] showed that for incorporation of levoglucosan into particles from AP ozonolysis at low RH, the uptake was kinetically limited with a measured diffusivity of 10^{-15} cm^2 s^{-1} corresponding to an equilibrium timescale for a 100 nm particle of ~10^3 s. Similarly, Han *et al.*[54] found that the uptake of dicarboxylic acids into SOA particles was hindered under high viscosity/low RH conditions because of slow diffusion in the particle phase. Zelenyuk *et al.*[55] showed that when SOA particles are exposed to polycyclic aromatic hydrocarbons (PAHs), the PAHs remain on the surface because of very slow diffusion into the particles, and their evaporation back to the gas phase is also relatively fast. By comparison, when PAHs are present *during* SOA formation, they remain trapped inside the SOA matrix, and their evaporation is hindered. Evidence of species trapped inside the SOA matrix has been reported previously in this and other laboratories.[33,41,47,55−57] The focus of the previous studies has been on inhibited evaporation of the trapped species, which has led to an estimation of diffusion coefficients in the range of 10^{-14} to 10^{-17} cm^2 s^{-1}.

A previous study by Vander Wall *et al.*[47] examined the incorporation of three organic nitrates (ON)—*β*-hydroxyhexyl nitrate (HHN), *β*-hydroxypropyl nitrate (HPN), and 2-ethylhexyl nitrate (2EHN)—into particles formed in a flow reactor from the ozonolysis of AP both *during* the particle formation and growth process as well as *after* growth. It was shown that partition coefficients ($K_{SOA} = [ON]_{SOA}/[ON]_{gas}$) were higher for ON incorporation *during* growth by factors of 3−15, and a kinetically-controlled burying mechanism was proposed to explain these results. However, the effects of different particle formation conditions are unknown.

Previous work has shown that SOA particle composition and properties such as volatility and viscosity can vary with particle size and mass loading.[58−64] Kourtchev *et al.*[65] found that the contribution of oligomers to the particle composition increased with AP concentration/particle mass loading. In the context of a burying mechanism,[47] if the oligomers formed in the gas phase are efficient burying species, increased oligomer formation may enhance the uptake of trace gases into the particles. The current study examines the incorporation of the three ON used in the previous studies[46,47] into particles during formation and growth from the ozonolysis of AP at varied initial concentrations of AP (between 100 and 1450 ppb) with a constant ozone concentration (250−300 ppb), and thus variable mass loadings, either with or without an OH scavenger. An updated version of the Master Chemical Mechanism (MCM v3.3.1)[66−68] including dimers and autoxidation processes[69] is also employed here to understand the distribution of gas-phase products under these reaction conditions.

EXPERIMENTAL SECTION

Aerosol Generation and Particle Size Distributions. Particles were generated in a large volume, slow flow aerosol flow reactor, as described in detail previously.[70] All organic reactants were introduced in the initial mixing section of the reactor. Gas-phase AP (ranging from 100 to 1450 ppb) was generated by injection of the pure liquid (Sigma-Aldrich, >99%) from an automated syringe pump (New Era Pump System Inc., Model NE-1000) into a stream of clean, dry air flowing at 10 L min^{-1}. When an OH scavenger was used, cyclohexane (CH, Fisher Scientific, 99.9%) was injected simultaneously with AP to produce a final CH concentration of 100 ppm in the flow reactor. Details on the gas-phase measurements for AP and CH are found in Supporting Information. Ozone was generated by flowing 0.4 L min^{-1} O_2 gas (Praxair, 99.993%) through a UV mercury pen lamp (UVP, Inc.) and was subsequently diluted with 9.6 L min^{-1} of air before being added to the first stage of the flow reactor (upstream of the organic reactants), with final concentrations in the flow reactor between 250 and 300 ppb O_3 measured using a photometric ozone analyzer (Advanced Pollution Instrumentation, Inc. model 400). An additional 14 L min^{-1} of air was introduced into the flow reactor to create a total flow rate of 34 L min^{-1}. Experiments were performed under dry conditions (RH < 5%) without seed particles, at ambient pressure and temperature (296−299 K).

One of three ON was introduced independently into the flow reactor by flowing 1 L min^{-1} air through a glass trap containing the individual pure liquid into a stream of air totaling 10 L min^{-1} simultaneously with AP, either with or without CH. While the alkyl nitrate 2EHN (Sigma-Aldrich, 97%) was used as purchased, two hydroxy nitrates, HPN and HHN (82−93% purity), were synthesized as described previously[46] using the method of Cavdar and Saracoglu.[71] Details on the gas-phase measurements for the ON are found in Supporting Information. The concentrations of each ON in the flow reactor after dilution were 5.7, 4.6, and 0.21 ppm for 2EHN, HPN, and HHN, respectively (Table 1).

Table 1. Relevant Properties of the Three Organic Nitrates

ON	molecular weight (g mol^{-1})	gas-phase concentration[a] in the flow reactor[b] (molecules cm^{-3} and ppm)	saturation vapor pressure (Pa, calculated using Moller[c] and SIMPOL.1[d])[46,47]
2EHN	175	$(1.4 \pm 0.1) \times 10^{14}$ cm^{-3}, 5.7 ± 0.1 ppm	14[c], 18[d]
HPN	121	$(1.1 \pm 0.1) \times 10^{14}$ cm^{-3}, 4.6 ± 0.1 ppm	24 ± 16[c], 16[d]
HHN	163	$(5.2 \pm 1.5) \times 10^{12}$ cm^{-3}, 0.21 ± 0.06 ppm	0.50 ± 0.21[c], 0.85[d]

[a]Error bars for the gas-phase concentration are ±1σ propagated from the average of three measurements out of the trap prior to dilution into the flow reactor. [b]Values were estimated by measuring the ON concentration directly out of the trap and accounting for the factor of 34 dilution into the flow reactor. While only diluted 2EHN was able to pass through the long sampling line to be measured directly by GC−MS, the estimated concentration for 2EHN agreed well with the GC−MS measurement. [c]Values estimated using Moller[102,103] for HPN and HHN are the average of the two isomers. Only one isomer is present for 2EHN. Error bars are ±1σ. [d]SIMPOL.1[104] does not distinguish between isomers.

The particles were sampled after 7 and 31 min reaction time, corresponding to the first and last port of the flow reactor. Particle size distributions were monitored using a scanning mobility particle sizer (SMPS, TSI) equipped with a ^{85}Kr neutralizer, a model 3080 classifier, a 3081 long differential mobility analyzer, and a 3776 butanol-based CPC, as well as an aerodynamic particle sizer (APS, TSI model 3321). Size distributions measured by both instruments were combined, and a Weibull 5-parameter fit[28,46] was used to estimate total mass loading. Note that for AP concentrations greater than 500 ppb, the addition of the APS data and a Weibull fit was necessary; however, the 100 ppb AP and 250 ppb AP

https://dx.doi.org/10.1021/acsearthspacechem.0c00163
ACS Earth Space Chem. 2020, 4, 1435−1447

conditions did not show a significant difference compared to that using the total mass concentration reported by the SMPS alone. Polydisperse particles were collected onto a germanium attenuated total reflectance Fourier transform infrared crystal at the end of the flow reactor (after 31 min reaction time) using a custom impactor with a 50% cut-off diameter of 240 nm for visual inspection of the impaction pattern, providing insight into the phase of the particles.[27]

Particulate ON Quantification and Partition Coefficient Calculation. A high-resolution time-of-flight aerosol mass spectrometer (HR-ToF-AMS, Aerodyne)[72−75] was used to characterize the bulk composition of the particles. Particles were sampled at a flow rate of ∼82 mL min^{-1} into the HR-ToF-AMS inlet and were focused with an aerodynamic lens, vaporized at 600 °C, and ionized *via* electron impact (EI, 70 eV) ionization. The data presented were acquired in the V-mode without HEPA-filter dilution and were analyzed using Igor Pro v. 6.37 (WaveMetrics, Inc.) with SQUIRREL (v. 1.62A) and PIKA (v. 1.22A), as done previously.[47] Elemental analysis was carried out using the default calibration values. To quantify the amount of ON in the particles, the HR-ToF-AMS mass concentrations of NO^+ and NO_2^+ ions were expressed as moles ON (n_{ON}) per L of SOA as described in eq 1:

$$[\mathrm{ON}]_{\mathrm{SOA}} = \frac{n_{\mathrm{ON}}}{\text{volume SOA}} = \frac{\left[\mathrm{NO}^+ \times \frac{1}{\mathrm{MW}_{\mathrm{NO}^+}}\right] + \left[\mathrm{NO_2}^+ \times \frac{1}{\mathrm{MW}_{\mathrm{NO_2}^+}}\right]}{\mathrm{HROrg}} \times d_{\mathrm{SOA}} \times \frac{\mathrm{RIE}_{\mathrm{Org}}}{\mathrm{RIE}_{\mathrm{ON}}} \quad (1)$$

Previous studies have shown that ON fragment in EI ionization to yield NO^+ and NO_2^+ as major fragments[76−80] with negligible $CHNO^+$ or CHN^+ fragments.[77,79] Thus, in eq 1, the mass loading of NO^+ (μg m^{-3} air) and NO_2^+ (μg m^{-3} air) are converted into moles m^{-3} of ON using the molecular weights of NO^+ and NO_2^+ (30 and 46 g mol^{-1}, respectively), assuming that each ON will give either an NO^+ or an NO_2^+ fragment. The mass concentration of SOA, taken as the total organic signal measured by the AMS, HROrg (μg m^{-3} air), is expressed as a volume concentration of SOA (L m^{-3} air) using its density (d = 1.2 × 10^3 g L^{-1}).[81] The default value for the relative ionization efficiency (RIE) of organics (1.4) was used for SOA, while an RIE of 1.0 was used for all ON.[82]

To calculate the partition coefficients, K_{SOA}, from the HR-ToF-MS measurements, eq 2 was used,

$$K_{\mathrm{SOA}} = \frac{[\mathrm{ON}]_{\mathrm{SOA}}}{[\mathrm{ON}]_{\mathrm{gas}}} \quad (2)$$

where the concentration of ON in the condensed phase, $[ON]_{SOA}$ (in moles L^{-1} SOA), from eq 1 was divided by the gas phase concentration $[ON]_{gas}$ in the flow reactor (in moles L^{-1} air). Gas phase concentrations (Table 1) for each nitrate were determined by gas chromatography−mass spectrometry (GC−MS) as discussed in Supporting Information.

Tandem Flow Tube Experiments (Uptake after Growth). Experiments exposing ON-free particles exiting the flow reactor to gas-phase ON *after* growth were also carried out following the procedure in Vander Wall *et al.* for 2EHN.[47] A schematic of the tandem flow tube setup is shown in Figure S1. Particles were generated from 250 ppb AP and 250 ppb O_3 with 100 ppm CH in the large flow reactor as described above. At the end of the flow reactor (after 31 min reaction time), the gases were removed using a monolith carbon denuder (NovaCarb, MAST Carbon, Ltd.) and a portion of the particle flow was directed through a smaller flow tube (∼0.4 L min^{-1}). Here, particles were exposed to concentrations of each ON individually at either near-saturation vapor pressure using an open reservoir containing the pure liquid placed inside the flow tube or at lower concentrations by flowing air over a trap containing the pure liquid located outside of the flow tube. In the latter case, the concentration of the ON is diluted upon entering the flow tube. The residence time in the small flow tube was ∼7 min, a similar timescale to the reaction time in the large flow reactor at sampling port 1. Particulate ON was quantified by HR-ToF-AMS as described above. Note that exposure to HHN in the small flow tube (which had a higher surface to volume ratio than the flow reactor) was not possible because of decomposition of the HHN on the walls of the flow tube. However, results from 2EHN and HPN are discussed.

Kinetic Modeling. A simplified kinetic model for the ozonolysis of AP was developed using Kintecus[83] to evaluate the extent of OH chemistry in the experiments (see Table S1). In addition, the gas-phase product distribution was modeled for each reaction condition with the OH scavenger using the MCM (http://mcm.york.ac.uk/) v3.3.1[66−68] and the AtChem box model.[84] For further analysis into the distribution of dimers across the reaction conditions studied here, the mechanism was updated to include highly oxidized multifunctional compounds (HOMs) and dimer formation, as well as RO_2 autoxidation, as described by Zhao *et al.*[69] The amount of reacted AP and ozone predicted by the MCM and the simplified Kintecus model agreed with each other within 2%.

Effective Net Uptake Coefficients. The number of collisions of a gas-phase oxidized organic molecule formed in the AP−ozone reaction with the particle surface relative to that of a gas phase ON molecule was used to lend insight into the burying mechanism as a function of changing gas phase concentrations and particle surface area using eq 3:

$$\frac{N_{\mathrm{ON}}}{N_{P_{\mathrm{SOA}}}} = \frac{\gamma_{\mathrm{ON}} \times [\mathrm{ON}]_{\mathrm{gas}} \times \sqrt{\frac{RT}{2\pi M_{\mathrm{ON}}}} \times A_{\mathrm{SOA}}}{\gamma_{P_{\mathrm{SOA}}} \times [P_{\mathrm{SOA}}]_{\mathrm{gas}} \times \sqrt{\frac{RT}{2\pi M_{P_{\mathrm{SOA}}}}} \times A_{\mathrm{SOA}}} \quad (3)$$

In eq 3, P_{SOA} is a proxy for all low volatility ozonolysis products that are taken up to grow the particles and N_{ON} and $N_{P_{SOA}}$ are the number of molecules of ON and molecules of P_{SOA} taken up per cm^3 air per second, respectively; γ is the effective uptake coefficient for each ON and for P_{SOA}; M is their respective molar mass ($M_{P_{SOA}}$ is taken as the average over all oxidation products forming SOA as 200 g mol^{-1});[85−87] and A_{SOA} is the surface area concentration of the SOA from the size distribution measurements (cm^2 m^{-3}). The gas-phase concentration of ON in the flow reactor ($[ON]_{gas}$, molecules cm^{-3}) is based on the GC−MS-determined concentration. The expression $\gamma_{P_{SOA}} \times [P_{SOA}]_{gas}$ (molecules cm^{-3}) in eq 3 is related to the uptake of oxidation product molecules from AP ozonolysis that form the SOA particles and is determined using the measured SOA mass loadings determined by SMPS (M_0, μg m^{-3}), following the conversion in eq 4,

$$\gamma_{P_{\mathrm{SOA}}} \times [P_{\mathrm{SOA}}]_{\mathrm{gas}} = M_0 \times \frac{1}{M_{P_{\mathrm{SOA}}} \times 10^6} \times N_{\mathrm{A}} \times 10^6 \quad (4)$$

https://dx.doi.org/10.1021/acsearthspacechem.0c00163
ACS Earth Space Chem. 2020, 4, 1435−1447

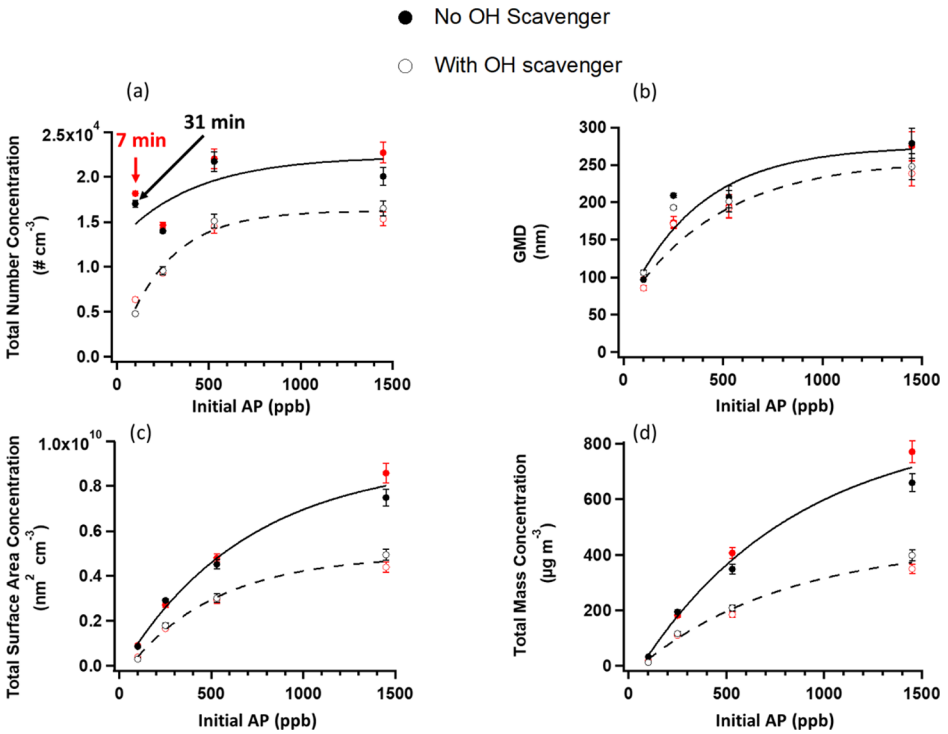

Figure 1. Typical particle (a) total number concentrations, (b) number-weighted GMD, (c) total surface area concentration, and (d) total mass concentration for particles formed either without the OH scavenger (closed circles) or with the OH scavenger (open circles), at 7 min (red) and 31 min (black) reaction time, formed without ON present. Error bars are $\pm 1\sigma$ from the average of three consecutive scans for the 100 and 250 ppb AP conditions, and ±5% applied to the Weibull fit for the higher concentrations. Solid lines (no OH scavenger) and dashed lines (with OH scavenger) are best fits to guide the eye.

where N_A is Avogadro's number and $M_{P_{SOA}}$ is the average molecular weight of the products composing SOA as described above.

The ratio $N_{ON}/N_{P_{SOA}}$ is also determined with eq 5 below

$$\frac{N_{ON}}{N_{P_{SOA}}} = \frac{N_{ON}}{N_{SOA}} = \frac{[ON]_{SOA}}{d_{SOA} \times \frac{1}{M_{SOA}}} \quad (5)$$

where the $[ON]_{SOA}$ (mol L^{-1} SOA) is determined experimentally from eq 1 using HR-ToF-AMS. It is assumed that $N_{P_{SOA}}$ is equal to N_{SOA}.

RESULTS AND DISCUSSION

Particle Size Distributions. Figure 1 shows typical values for the total number concentration (a), number-weighted geometric mean diameter (GMD) (b), total surface area concentration (c), and total mass concentration (d) for particles formed from AP and O_3 either with or without the OH scavenger. Using kinetics modeling,[47,83] the predicted steady-state OH concentrations at 7 min reaction time were $(3-8) \times 10^6$ with no OH scavenger and $(0.5-2) \times 10^5$ in the presence of the OH scavenger. The corresponding particle number distributions are shown in Figure S2 at 7 and 31 min reaction time. In all cases, there is little evolution of the size distributions between 7 and 31 min reaction time. This may reflect a balancing of continued formation of particles and their simultaneous wall loss.

When particles are formed in the presence of 100 ppm CH as an OH scavenger (Figure 1, open circles), the total particle number concentrations drop for all concentrations of AP (along with the corresponding mass and surface area concentrations), but the particle diameters do not significantly change compared to those without the OH scavenger. This is consistent with previous studies that showed OH scavengers can reduce the total number of particles formed by reducing the formation of HOMs.[88−90] By suppressing the formation of potential particle nucleating species such as HOMs, the total particle number decreased, but under conditions where the growth process remained the same, the particles reached the same GMD, consistent with the results observed here.

Two trends are evident as initial AP concentration increases. First, when experiments are performed in the absence of the OH scavenger (closed circles), the total number concentration increases only slightly, and the particles grow as indicated by the increase in GMD (~100 nm at 100 ppb AP *vs* ~250 nm at 1450 ppb AP), leading to an increase in total mass and surface area. Thus, as the concentration of AP increases in the absence of a scavenger, the concentrations of its oxidation products that are responsible for particle growth also increase. Second, in the presence of CH, total number and GMD (and thus surface area and mass) increase with the AP concentration, indicating that both new particle formation and growth are occurring.

Figure S3 shows the particle size distributions for SOA alone, upon addition of each ON, and after the OH scavenger is added. The ON themselves can act as OH scavengers, and in the case of 2EHN and HHN, their rate constants with OH are comparable to that of CH with OH (Table S1). Of the three ON, 2EHN has the highest OH rate constant and the largest gas-phase concentration. These two factors result in the most prominent change in the particle size distribution upon addition of 2EHN to the system. Second, HPN has a similar gas-phase concentration to 2EHN but a smaller OH rate constant, and so the change in the particle size distribution

https://dx.doi.org/10.1021/acsearthspacechem.0c00163
ACS Earth Space Chem. 2020, 4, 1435−1447

upon addition of HPN was less drastic than for 2EHN. Lastly, HHN has a similar OH rate constant to 2EHN but has a much smaller gas phase concentration, so there was no evident change in the size distribution upon addition of HHN. The size distributions show that the impacts of adding an ON are, in some cases, similar to those of adding an OH scavenger, which has implications for the ON content in the particles as discussed later.

SOA particles from the ozonolysis of AP under dry conditions have previously been shown to be highly viscous or semisolid in phase.[26−28,31−38,40,42,53−55] High concentrations of ON have previously been shown to have a plasticizing effect on the SOA, and equilibrium with the gas phase was achieved upon introduction of saturation vapor pressures of the three ON on the timescale of ∼4−20 min.[46] However, the concentrations used in the flow reactor are over 30 times smaller and did not induce a significant plasticizing effect in our previous study using initial conditions of 250 ppb of both AP and O_3.[47] More details on the phase of these particles are found in Supporting Information (Figures S4 and S5).

Particulate ON Concentrations in the Absence of an OH Scavenger. Figure 2a shows the HR-ToF-AMS-measured concentration of condensed phase ON ($[ON]_{SOA}$, moles per L of SOA) as a function of initial AP concentration in the absence of an OH scavenger at 7 min reaction time, calculated using eq 1. Similar values were obtained for particles measured at 31 min. For 2EHN in the absence of a scavenger, the amount of ON that is observed in the particles decreases as the initial concentration of AP increases. The OH rate constant for 2EHN (Table S1) is sufficiently high that it can react to form lower volatility oxidation products retaining the $-ONO_2$ moiety[47] that can partition into the SOA. The initial first-order rates of loss due to reaction with OH, estimated as $k[X]_0$, where X is AP or 2EHN, reveal the likelihood of 2EHN acting as an OH scavenger at each condition. For the lowest initial concentration of AP ($[AP]_0$ = 100 ppb), 2EHN acts as an efficient OH scavenger itself as its initial loss rate ($k[2EHN]_0$ = 8.8 × 10^2 s^{-1}) is almost seven times higher than that of AP ($k[AP]_0$ = 1.3 × 10^2 s^{-1}), consistent with the change in the particle size distribution seen in Figure S3. For the higher concentrations of AP ($[AP]_0$ = 1450 ppb), the initial rate of 2EHN is ∼0.5 times that of AP ($k[AP]_0$ = 1.9 × 10^3 s^{-1}). Thus, as the initial concentration of AP increases, OH preferentially reacts with AP instead of 2EHN, and as a result, fewer multifunctional lower volatility oxidation products deriving from the parent ON are formed and taken up into the particles, consistent with the trend in Figure 2.

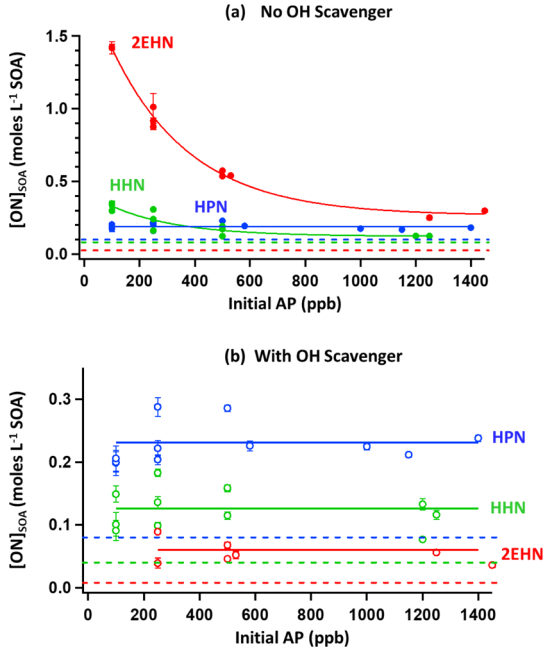

Figure 2. Moles of ON per liter of SOA ($[ON]_{SOA}$, determined from the HR-ToF-AMS) for particles formed in the presence of 5.7 ppm 2EHN, 4.6 ppm HPN, or 0.21 ppm HHN, (a) in the absence of the OH scavenger and (b) in the presence of 100 ppm CH, at 7 min reaction time. Error bars are ±2σ from the absolute uncertainty in the AMS. Solid lines are best fits to the data points to guide the eye in (a) and in (b) are the average moles ON per liter SOA across the reaction conditions. Dashed lines are the expected values if equilibrium partitioning from uptake into thin films of impacted particles held.[45,46] The 2EHN signal in the particles in (b) was not detectable at 100 ppb initial AP.

A similar trend is seen in Figure 2a for HHN, but to a much lesser extent. The initial first order rate of loss due to reaction with OH is 27 s^{-1} for HHN and is less than that of AP across all the conditions in Figure 2a. At 100 ppb AP, the initial rate of AP loss due to OH reaction is ∼5 times higher than the rate of HHN loss, and it increases up to ∼80 times higher for ∼1.5 ppm AP. Thus, for the lowest concentration of AP, some of the OH is still able to react with HHN to form lower volatility oxidation products (with a retained $-ONO_2$ functional group[47]) that are incorporated into the particles. Therefore, there is slightly more ON taken up in this condition when compared to the higher concentrations of AP in the presence of HHN.

For HPN, the amount of ON taken up into the particles is unaffected by the concentration of AP (Figure 2a). The initial rate of loss due to reaction with OH is 1.9 × 10^2 s^{-1} for HPN (compared to 1.3 × 10^2 s^{-1} for 100 ppb AP). Consistent with these comparable loss rates with OH, there is a change in the particle size distributions in the presence of HPN at the smallest AP concentration (Figure S3), reflecting a smaller contribution of OH + AP chemistry to particle growth. However, as discussed previously by Vander Wall *et al.*,[47] the products of the HPN reaction with OH are likely to be small and more volatile and are not expected to be incorporated into the SOA.

In summary, the measurements of condensed phase ON in the absence of an OH scavenger indicate that under each initial AP condition, different amounts of (unidentified) multifunctional ON oxidation products retaining the $-ONO_2$ functional group are taken up into the particles. However, in the presence of an OH scavenger, the parent ON is the only ON species taken up, and thus these scavenger experiments can be used to determine partition coefficients for the three parent ON.

Partition Coefficients and Particle Composition in the Presence of an OH Scavenger. When an OH scavenger is present, the contribution of ON + OH reaction products to the particulate ON signal is small. From kinetics modeling[47,83] at 7 min reaction time, less than 0.03% of HPN, 0.10% of HHN, and 0.11% of 2EHN reacts with OH when 100 ppm CH is present at all AP concentrations (compared to 0.3% of HPN, 1.5% of HHN, and 0.83% of 2EHN when no OH scavenger is present), and thus the ON in the particles is attributed to the parent ON. Figure 2b shows the measured concentrations of the ON in SOA in the presence of CH. Under these

https://dx.doi.org/10.1021/acsearthspacechem.0c00163
ACS Earth Space Chem. 2020, 4, 1435−1447

conditions, no trends are apparent across the range of AP concentrations, with the exception of 2EHN which is not detected at the lower AP concentration (100 ppb). With that exception, it is important to note that for all three nitrates, the concentration of the nitrate taken up by the particles is higher than that estimated from equilibrium partitioning into thin films of impacted particles (dashed lines in Figure 2, determined after accounting for the difference in gas-phase ON concentration between the flow reactor and thin-film experiments).[47]

Effective partition coefficients, K_{SOA}, were calculated using eq 2 and are shown in Figure 3 for all three ON across all

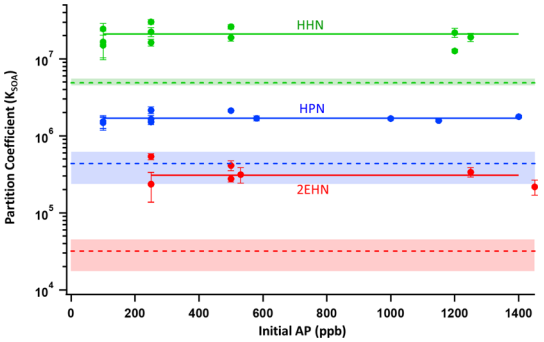

Figure 3. Partition coefficients (K_{SOA}) for particles formed from AP ozonolysis in the presence of 100 ppm CH as an OH scavenger and 5.7 ppm 2EHN, 4.6 ppm HPN, or 0.21 ppm HHN. Error bars are $\pm 2\sigma$ from the absolute uncertainty in the HR-ToF-AMS. The dashed lines show the partition coefficients measured for the equilibrium partitioning of ~190 ppm 2EHN, ~ 160 ppm HPN, or ~7 ppm HHN into thin films of particles formed from 250 ppb AP and 100 ppm CH, with shaded boxes showing $\pm 1\sigma$ from the average of at least three experiments.[46] The 2EHN signal in the particles was not detectable at 100 ppb initial AP.

initial concentrations of AP. Also shown in Figure 3 are the partition coefficients determined for equilibrium partitioning of ON into thin films of impacted particles formed from 250 ppb AP and 100 ppm CH (dashed lines).[47] For all ON, there was no distinct trend in the partition coefficient across all AP concentrations, apart from the partitioning of 2EHN into SOA formed from 100 ppb AP which was not detectable. The average partition coefficients across all measurable conditions were found to be $(3.1 \pm 0.4) \times 10^5$ for 2EHN, $(1.7 \pm 0.2) \times 10^6$ for HPN, and $(2.1 \pm 0.3) \times 10^7$ for HHN ($\pm 1\sigma$), indicated by the solid lines in Figure 3. Note that these are significantly higher than the values measured previously[47] for equilibrium partitioning into thin films shown by the dashed lines in Figure 3. This enhanced partitioning, interpreted as burying of ON within SOA particles as they form, is explored as a function of initial AP below.

Previously, Vander Wall *et al.*[47] studied the exposure to 2EHN *after* growth of particles formed from 250 ppb AP in the presence of CH as an OH scavenger (Figure S1). These studies showed that the amount of 2EHN in the particles was undetectable in the time frame of 7 min at a similar gas-phase concentration to those used in the flow reactor. Similar results were obtained here when particles formed under the same conditions were exposed to ~6.5 ppm of gas-phase HPN in the small flow tube for 7 min, again resulting in undetectable levels of particulate ON. This indicates that in the large flow reactor, the detectable ON in the particles during growth was still above the expected equilibrium partitioning value.

SOA particles from AP ozonolysis are known to become less viscous when formed at higher initial AP concentrations or higher mass loadings.[61,91] Thus, if equilibrium partitioning were to be reached, it would be more probable for particles formed at the higher initial AP concentrations. However, not only were all the average experimental partition coefficients nearly constant and greater than the corresponding equilibrium constants, SOA particles formed in the current study were also observed to exhibit significant bounce patterns in the impactor, especially at the higher initial AP concentrations (Figure S4). Furthermore, the SOA particles with ON incorporated in them also exhibited clear bounce patterns, including at the higher initial AP concentrations (Figure S5). Although some changes in the amount of bounce were seen from variation in total impacted mass because of lower particle concentrations when OH was scavenged and smaller particle diameters/mass loadings at the smallest concentrations of AP, the particles formed across all conditions studied here remain highly viscous as discussed in Supporting Information. Additionally, Vander Wall *et al.*[47] showed in a previous study that the partition coefficients for these ON incorporated into particles *during* growth (at 250 ppb $[AP]_0$) were higher than the equilibrium partition coefficients for these nitrates into thin films of impacted particles (*i.e., after* growth) that reached equilibrium between ~4 and 18 min with gas-phase concentrations near the saturation vapor pressure.

Another possible explanation for the constant partition coefficients as a function of initial AP concentration could be that the relative rate of uptake for the ON and the gaseous ozonolysis products, represented by P_{SOA}, remains constant. P_{SOA} designates all products derived from the ozonolysis of AP that contribute to particle formation and growth and is representative of what forms the SOA. As the concentration of AP increases, the concentration of P_{SOA} is anticipated to increase. Thus, the number of collisions of P_{SOA} per cm^2 of particle surface area, and hence its net uptake, will increase (creating higher SOA mass loading). However, the ON collisions per cm^2 of particle surface area should remain the same because the ON gas phase concentrations remain constant. One might expect that as more P_{SOA} collides and is taken up into the particles, the particulate ON signal per L of SOA would decrease because of dilution according to eq 3 (assuming γ_{ON} remains constant). This contrasts with the observed constant ON concentration in SOA across the studied reaction conditions and initial AP concentrations when OH is scavenged (Figure 2b). However, if P_{SOA} contributes to the incorporation of ON by acting as a burying species, as the concentration of P_{SOA} increases, the trapping of ON in the particles will also increase (and thus γ_{ON} will increase). This counterbalances the effects of dilution and results in a constant particulate ON concentration.

To explore this in more detail, the effective uptake coefficients for the ON were estimated using eqs 3−5 and the average ON concentration per L of SOA (Figure 2b). Figure 4 shows that the effective net uptake coefficients for the incorporation of the ON into the particles (γ_{ON}) increased with initial AP concentrations, ranging from $(2 \text{ to } 5) \times 10^{-5}$ for 2EHN, $(0.1 \text{ to } 3) \times 10^{-4}$ for HPN, and $(0.2 \text{ to } 4) \times 10^{-3}$ for HHN. In the absence of any P_{SOA} from the ozonolysis of AP (*i.e.,* as $[P_{SOA}]_g$ approaches 0 ppb), the uptake coefficient is expected to be γ_{ON} for the ON alone based solely on the

https://dx.doi.org/10.1021/acsearthspacechem.0c00163
ACS Earth Space Chem. 2020, 4, 1435−1447

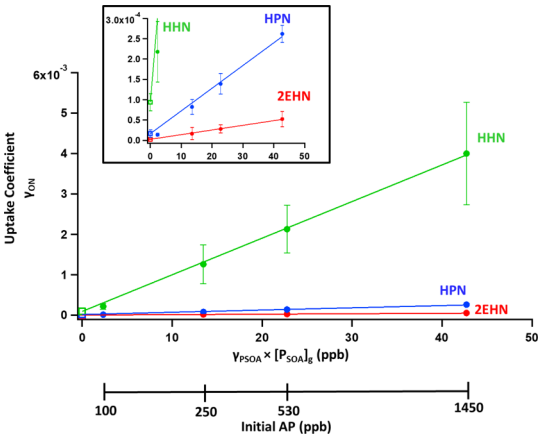

Figure 4. Effective uptake coefficients (γ_{ON}) for the uptake of ON into the particles (γ_{ON}) *vs* the product of the uptake coefficient ($\gamma_{P_{SOA}}$) and the concentration of P_{SOA} (ppb). The inset shows an expanded view for HPN and 2EHN. The open boxes at $\gamma_{P_{SOA}} \times [P_{SOA}]_g = 0$ are the uptake coefficient measured from thin films of impacted particles.[46,47] Error bars are $\pm 1\sigma$ propagated from the average of at least three experiments. Lines are linear fits to the data points.

number of collisions with the particle surface per cm^2 (in the absence of any enhancement due to burying), which was the measured uptake coefficient onto thin films of impacted particles.[46,47] The values for thin film γ_{ON} are $(2.6 \pm 1.0) \times 10^{-6}$ for 2EHN, $(1.7 \pm 0.9) \times 10^{-5}$ for HPN, and $(9.4 \pm 2.1) \times 10^{-5}$ for HHN ($\pm 1\sigma$). They are included as the *y*-intercept in Figure 4 and are in good agreement with the trends in uptake coefficients determined here. This analysis conveys the ability of the burying mechanism to increase uptake beyond that which is expected to occur through collisional uptake alone. However, it ignores potential changes in gas and particle phase composition which are examined below.

The effectiveness of burying the ON depends not only on the concentration of P_{SOA} but also on the nature of P_{SOA} as a burying species, which may vary depending on the reaction conditions. Claflin *et al.*[59] showed that SOA formed at low RH under a high-[VOC] condition (1 ppm AP, 2 ppm O_3) had a different distribution of functional groups than SOA formed under a low-[VOC] condition (10 ppb AP, 300 ppb O_3), with the latter having a higher contribution from peroxides while most other functional groups were higher in the former scenario. Additionally, Molteni *et al.*[60] showed that the distribution of highly oxygenated organic molecules (HOMs) varied with the reaction conditions, and larger contributions from dimers occurred at higher initial AP concentrations as more AP reacted.

To probe this for the reaction conditions studied here, the MCM (v3.3.1)[66−68] was used to predict changes in the product distribution. An updated mechanism[69] was used that includes dimer formation from RO_2-RO_2 chemistry, where the RO_2 is produced from oxidation steps within the original MCM (*e.g.*, Criegee intermediate decomposition in the absence of OH) as well as autoxidation processes producing more highly oxidized RO_2 species. As the initial concentration of AP increases and more AP is reacted away, the total amount of products also increases, with or without the addition of dimers to the mechanism (Figure 5a,b). The total concentration of all products predicted by the MCM with dimers added, and the concentrations of the $C_{10}-C_{20}$ products are listed in Table 2. Across all conditions, there were only small changes in the distribution of the products, as shown in Figure 5c. The $C_{10}-C_{20}$ products systematically comprised ~24−27% of the overall product distribution. The distribution of the $C_{14}-C_{20}$ dimer species is shown in Figure S6, along with the dimer yield (the concentration of dimers formed relative to the

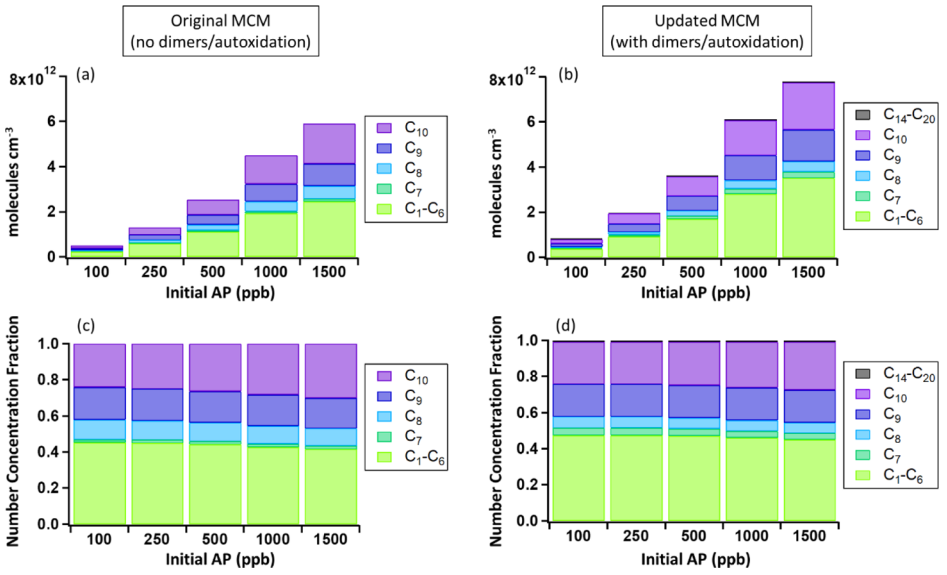

Figure 5. AP oxidation product distribution from the MCM after 7 min reaction in the presence of CH (100 ppm) separated by carbon number. (a) Stable gas phase molecules formed based on the original MCM mechanism, (b) stable gas phase molecules formed using the updated MCM mechanism including autoxidation processes and the formation of dimers, (c) normalized fraction of stable products without dimers (original MCM mechanism), and (d) normalized fraction of stable products with dimers added. The updated MCM uses rate constants for the C_7-C_{10} RO_2 cross reactions of 2×10^{-12} cm^3 $molecule^{-1}$ s^{-1} for the OH-derived RO_2 and 7.5×10^{-13} cm^3 $molecule^{-1}$ s^{-1} for the Criegee-derived RO_2, with an applied yield of 4% for the dimer formation reactions, and autoxidation rate constants of 1 and 3 s^{-1} for the Criegee-derived and OH-derived RO_2, respectively.[68]

https://dx.doi.org/10.1021/acsearthspacechem.0c00163
ACS Earth Space Chem. 2020, 4, 1435−1447

Table 2. Concentrations (ppb) of Stable Gas-Phase Products Formed, Predicted by the MCM with Dimer Formation Added

$[AP]_0$ (ppb)	MCM predicted C_1−C_{20} products (ppb)	MCM predicted C_{10}−C_{20} products (ppb)	% C_{10}−C_{20} of total (%)
100	33	7.9	24
250	79	19	24
500	147	36	25
1500	317	87	27

amount of AP reacted) which is ∼1% across all conditions. These results indicate that the relative fractions of potential burying candidates do not change significantly, consistent with a similar bulk composition and the observed partition coefficients across all initial AP conditions.

Although only relatively small changes were predicted in the overall product distribution (in terms of number of carbons per molecule), some changes in composition were predicted from the MCM results when the level of oxidation was taken into account. Figure S7 shows the distribution of $C_{10}H_xO_y$ products separated by the number of oxygens for all conditions when autoxidation/dimer formation was added into the MCM. As the concentration of AP increases, the contribution of more-oxygenated species such as $C_{10}H_xO_{10}$ decreases (from 19% at 100 ppb AP to 11% at 1.5 ppm AP), while the contribution of less-oxygenated $C_{10}H_xO_2$ increases (from 1 to 16%). However, the majority (∼60%) of the C_{10} species consist of $C_{10}H_xO_3$−$C_{10}H_xO_5$ across the conditions. Thus, the steady increase in concentrations of products that bury the ON is likely more important than the changes in product distributions.

Relative Timescales of ON Burying. If the particle growth observed in the abovementioned experiments is due to a kinetic burying mechanism, an incoming ON molecule must reside on the surface for sufficient time such that a colliding, low volatility ozonolysis product (P_{SOA}) can efficiently bury it. The collision frequency of P_{SOA} with the particle surface can be estimated using gas kinetic theory and eq 6

$$\text{collision frequency } (\text{cm}^{-2}\ \text{s}^{-1}) = [P_{SOA}]_{gas} \times \sqrt{\frac{RT}{2\pi M_{P_{SOA}}}} \quad (6)$$

where $[P_{SOA}]_g$ is the subset of ozonolysis products that are taken up to form and grow the SOA particle matrix, and $M_{P_{SOA}}$ is the average molecular weight of P_{SOA} (assumed to be 200 g mol^{-1}).[85,86] The $[P_{SOA}]_g$ was estimated from the $\gamma_{P_{SOA}} \times [P_{SOA}]_{gas}$ using eq 4 and the measured SOA mass loading (M_0, $\mu g\ m^{-3}$), assuming a $\gamma_{P_{SOA}}$ of one. Taking the inverse of the collision frequency as an estimate of the time between collisions of a burying P_{SOA} species with one cm^2 of particle surface, this time can be calculated. Using $\gamma_{P_{SOA}} = 1$ provides a reference base. Figure S8 shows the time between collisions of P_{SOA} with the particle surface based on $\gamma_{P_{SOA}} = 1$ (which we refer to as relative time) and normalized to that estimated for 100 ppb AP (∼8×10^{-3} s).

As expected, the relative time between collisions of a burying species with the particles is much larger at 100 ppb AP than it is for the other reaction conditions/initial concentrations of AP, ∼6 times longer than that for the 250 ppb AP and higher conditions. This means that at the lower AP concentrations, the ON has to have a longer residence time on the surface in order to be buried by incoming P_{SOA}. The hydroxy nitrates were taken up at all reaction conditions, indicating that the average residence time for the HPN and HHN on the particle surface was sufficiently long that they could be buried by an incoming P_{SOA} molecule.

HR-ToF-AMS was used to detect changes in particle composition. The average O/C ratio of the SOA slightly decreased from 0.46 at 100 ppb to relatively constant values of 0.43−0.42 as the AP initial concentration increased to 1450 ppb, though the overall change was small, as shown in Table 3.

Table 3. Oxygen-to-Carbon Ratio Measured by AMS for SOA Formed in the Flow Reactor in the Presence of an OH Scavenger and the Concentrations of AP Reacted at 7 min Reaction Time[a]

$[AP]_0$ (ppb)	ΔAP (ppb)	O/C (±1σ)
100	45−74	0.46 ± 0.01
250	90−153	0.43 ± 0.02
500−530	75−185	0.43 ± 0.02
700−1450	155−194	0.42 ± 0.01

[a]Error bars are ±1σ from the average of three experiments.

Figure S9 shows the intensity ratio of CO_2^+ (m/z 44) to either $C_4H_7^+$ (m/z 55, Figure S9a) or $C_2H_3O^+$ (m/z 43, Figure S9b), as a function of initial AP concentration, as well as the ratio of CO_2^+ to HROrg plotted against the ratio of $C_2H_3O^+$ to HROrg (Figure S9c). CO_2^+ is an indicator of more-oxygenated species such as acids and peroxides,[51,92,93] while $C_4H_7^+$ and $C_2H_3O^+$ are indicators of less-oxygenated species within the particles.[94] While there was little change from 250 ppb AP and higher, the 100 ppb AP condition exhibited a larger contribution from the more-oxygenated CO_2^+ fragment.

The change in the average O/C is consistent with the MCM predictions and other observations at variable AP concentrations and mass loadings. For example, Shilling *et al.*[58] showed that for SOA particles formed from AP ozonolysis using 1-butanol as an OH scavenger, the changes in the particle O/C and composition were more pronounced at smaller mass loadings, with higher O/C as the mass loading decreased, in agreement with the results shown here. The slightly more-oxygenated composition at 100 ppb AP could be consistent with the decrease in the partition coefficient of 2EHN, the least-oxygenated ON studied here. 2EHN should have a smaller affinity for these particles because of its less-polar alkyl nature and smaller hydrogen-bonding capacity compared to the hydroxy-nitrates,[46] which may result in insufficient surface residence time to be incorporated into the particles by a burying species at 100 ppb AP. HHN and HPN are more oxygenated with larger hydrogen-bonding capacities, and thus may have a stronger interaction with the particles such that they did not show this change at the lowest concentration of AP.

The results here indicate that the interaction of gaseous species with highly viscous SOA particles in the atmosphere depends on both the nature of the gas phase and that of the particle phase. The formation of large, low volatility species in the gas phase can facilitate the incorporation of more volatile molecules at amounts greater than expected based on equilibrium partitioning through a kinetically controlled burying mechanism. Figure 6 depicts such a mechanism for a semisolid particle, where a gas-phase molecule (G, such as an

https://dx.doi.org/10.1021/acsearthspacechem.0c00163
ACS Earth Space Chem. 2020, 4, 1435−1447

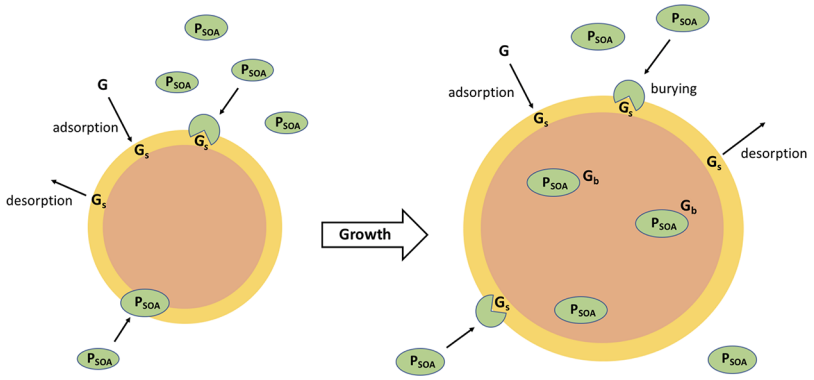

Figure 6. Schematic of the interactions between gas-phase species (G), representative of the ON in our study with an SOA particle. Once G is on the particle surface (G_s), the burying species (P_{SOA} oxidation products from AP ozonolysis) facilitates the incorporation of G into the particle (G_b) by hindering desorption/re-evaporation.

ON) is adsorbed on the surface of an SOA particle for sufficient time that it can be buried by an incoming P_{SOA} molecule (such as an oxidation product from AP). This burying process is in competition with scattering or desorption/evaporation. The burying mechanism can help trap the ON within the particle, reducing its re-evaporation into the gas phase and thus incorporating more within the particle phase than would be expected based on equilibrium partitioning.

CONCLUSIONS

Incorporation of several gaseous tracer molecules into viscous AP ozonolysis SOA particles serves as a probe to identify a burying mechanism occurring during particle growth under a range of SOA precursor concentrations. Results from this study show that OH radicals from the initial O_3 + AP reaction can increase the total amount of ON incorporated in the SOA particles through the formation of lower volatility multifunctional ON products. In the presence of an OH scavenger, the partition coefficients of all three parent ON were larger than expected from equilibrium partitioning, with no dependence on precursor AP concentration/particle mass loading. The exception was 2EHN, which was undetectable in the particles at the lowest concentration of AP studied here. Effective uptake coefficients for the incorporation of the ON into particles (γ_{ON}) increased with AP concentration and particle mass loading. Model studies predicted that while the distribution of gas-phase ozonolysis products did not significantly change across the conditions studied here, the total concentration of those products increased with the AP concentration, as expected. The similar partition coefficients across the conditions together with the increase in effective uptake coefficients for the ON can be explained by a kinetically controlled burying mechanism. The nature of the interaction between the gas-phase molecule and the surface of the particle will play a significant role in the uptake. At 100 ppb AP, for example, the less polar alkyl nitrate 2EHN was not quantifiable in the particles, indicating a smaller affinity for these particles which were found to be smaller and more oxygenated than particles formed at the other conditions.

Up to 90% of organic aerosol in the global troposphere is formed from atmospheric oxidation of VOCs and subsequent growth,[94−98] and much of this SOA consists of highly viscous particles, increasing in viscosity from the surface to the upper troposphere.[25] Burying of semivolatile compounds into particles as they form and grow could provide an important additional growth mechanism to air quality models in regions with high biogenic VOC concentrations. While tropospheric concentrations are much lower than those used in these laboratory experiments, a large number of biogenic and anthropogenic VOCs are available in air that also contribute to particle growth. The majority of air quality models employ equilibrium gas−particle partitioning to determine gas and particle interactions, assuming the particles are low viscosity liquids.[18] However, improvements in particle growth predictions have been reported when kinetically controlled condensation is included with equilibrium partitioning, especially under conditions of low RH and temperature.[99] The burying effect presented here over a wide range of initial AP concentrations leads to enhancements in equilibrium partitioning coefficients by factors of ∼4−10 under dry conditions at varied initial AP concentrations. While the presence of water vapor is expected to decrease particle viscosity and thus limit the enhancement of partitioning *via* this burying mechanism, it has been shown that SOA can remain highly viscous up to ∼70% RH or higher in laboratory[27] and field[34,100,101] studies. Further studies are warranted to explore additional atmospheric conditions.

ASSOCIATED CONTENT

Supporting Information

The Supporting Information is available free of charge at https://pubs.acs.org/doi/10.1021/acsearthspacechem.0c00163.

Additional details on the experimental methods and additional data supporting the main conclusions of the text; schematic of the tandem flow tube experiments (Figure S1); simplified kinetic reaction mechanism (Table S1); particle size distributions for SOA formed with or without OH scavenger in the absence of ON (Figure S2) and in the presence of ON (Figure S3); typical impaction pattern photographs of the impacted particles with or without OH scavenger in the absence of ON (Figure S4); typical impaction pattern photographs of the impacted particles with or without an OH scavenger in the presence of ON (Figure S5); concentration of C_{14}−C_{20} dimers predicted by the updated MCM mechanism (Figure S6); speciation of the C_{10} species predicted by the MCM mechanism (Figure S7); relative time between collisions for an

https://dx.doi.org/10.1021/acsearthspacechem.0c00163
ACS Earth Space Chem. 2020, 4, 1435−1447

incoming P_{SOA} burying species (Figure S8); AMS fragment ratios $CO_2^+/C_4H_7^+$ and $CO_2^+/C_2H_3O^+$ as a function of initial AP, and CO_2^+/HROrg vs $C_2H_3O^+$/HROrg (Figure S9) (PDF)

AUTHOR INFORMATION

Corresponding Author

Barbara J. Finlayson-Pitts − *Department of Chemistry, University of California Irvine, Irvine, California 92697-2025, United States;* orcid.org/0000-0003-4650-168X; Phone: (949) 824-7670; Email: bjfinlay@uci.edu; Fax: (949) 824-2420

Authors

Allison C. Vander Wall − *Department of Chemistry, University of California Irvine, Irvine, California 92697-2025, United States*

Lisa M. Wingen − *Department of Chemistry, University of California Irvine, Irvine, California 92697-2025, United States;* orcid.org/0000-0001-5847-9913

Véronique Perraud − *Department of Chemistry, University of California Irvine, Irvine, California 92697-2025, United States;* orcid.org/0000-0003-1247-9787

Yue Zhao − *School of Environmental Science and Engineering, Shanghai Jiao Tong University, Shanghai 200240, China;* orcid.org/0000-0003-1157-5101

Complete contact information is available at: https://pubs.acs.org/10.1021/acsearthspacechem.0c00163

Notes

The authors declare no competing financial interest.

The full updated MCM mechanism is publicly available and archived at https://doi.org/10.7280/D1M67M.[105]

ACKNOWLEDGMENTS

This work was funded by the NSF (Grant #1647386), the NSF Major Research Instrumentation (MRI) program (Grants #1337080 and #0923323), and the Army Research Office (Grant #W911NF1710105). The authors thank M. J. Ezell for assistance with the manuscript and helpful discussions.

REFERENCES

(1) Ziemann, P. J.; Atkinson, R. Kinetics, products, and mechanisms of secondary organic aerosol formation. *Chem. Soc. Rev.* **2012**, *41*, 6582−6605.

(2) Hallquist, M.; Wenger, J. C.; Baltensperger, U.; Rudich, Y.; Simpson, D.; Claeys, M.; Dommen, J.; Donahue, N. M.; George, C.; Goldstein, A. H.; Hamilton, J. F.; Herrmann, H.; Hoffmann, T.; Iinuma, Y.; Jang, M.; Jenkin, M. E.; Jimenez, J. L.; Kiendler-Scharr, A.; Maenhaut, W.; McFiggans, G.; Mentel, T. F.; Monod, A.; Prévôt, A. S. H.; Seinfeld, J. H.; Surratt, J. D.; Szmigielski, R.; Wildt, J. The formation, properties and impact of secondary organic aerosol: current and emerging issues. *Atmos. Chem. Phys.* **2009**, *9*, 5155−5236.

(3) Singh, A.; Bloss, W. J.; Pope, F. D. 60 years of UK visibility measurements: impact of meteorology and atmospheric pollutants on visibility. *Atmos. Chem. Phys.* **2017**, *17*, 2085−2101.

(4) Hinds, W. C. *Aerosol Technology: Properties, Behavior, and Measurement of Airborne Particles*; John Wiley & Sons, 1982.

(5) Finlayson-Pitts, B. J.; Pitts, J. N. *Chemistry of the Upper and Lower Atmosphere: Theory, Experiments, and Applications*; Academic Press, 2000.

(6) Seinfeld, J. H.; Pandis, S. N. *Atmospheric Chemistry and Physics: From Air Pollution to Climate Change*; Wiley, 2006.

(7) Fuzzi, S.; Andreae, M. O.; Huebert, B. J.; Kulmala, M.; Bond, T. C.; Boy, M.; Doherty, S. J.; Guenther, A.; Kanakidou, M.; Kawamura, K.; Kerminen, V.-M.; Lohmann, U.; Russell, L. M.; Pöschl, U. Critical assessment of the current state of scientific knowledge, terminology, and research needs concerning the role of organic aerosols in the atmosphere, climate, and global change. *Atmos. Chem. Phys.* **2006**, *6*, 2017−2038.

(8) Kanakidou, M.; Seinfeld, J. H.; Pandis, S. N.; Barnes, I.; Dentener, F. J.; Facchini, M. C.; Van Dingenen, R.; Ervens, B.; Nenes, A.; Nielsen, C. J.; Swietlicki, E.; Putaud, J. P.; Balkanski, Y.; Fuzzi, S.; Horth, J.; Moortgat, G. K.; Winterhalter, R.; Myhre, C. E. L.; Tsigaridis, K.; Vignati, E.; Stephanou, E. G.; Wilson, J. Organic aerosol and global climate modelling: a review. *Atmos. Chem. Phys.* **2005**, *5*, 1053−1123.

(9) Pope, C. A.; Dockery, D. W. Health effects of fine particulate air pollution: lines that connect. *J. Air Waste Manage. Assoc.* **2006**, *56*, 709−742.

(10) Mauderly, J. L.; Chow, J. C. Health effects of organic aerosols. *Inhalation Toxicol.* **2008**, *20*, 257−288.

(11) Heal, M. R.; Kumar, P.; Harrison, R. M. Particles, air quality, policy and health. *Chem. Soc. Rev.* **2012**, *41*, 6606−6630.

(12) Nel, A. Air pollution-related illness: effects of particles. *Science* **2005**, *308* (5723), 804−806.

(13) Hamra, G. B.; Guha, N.; Cohen, A.; Laden, F.; Raaschou-Nielsen, O.; Samet, J. M.; Vineis, P.; Forastiere, F.; Saldiva, P.; Yorifuji, T.; Loomis, D. Outdoor particulate matter exposure and lung cancer: a systematic review and meta-analysis. *Environ. Health Perspect.* **2014**, *122*, 906−911.

(14) Mannucci, P. M.; Harari, S.; Martinelli, I.; Franchini, M. Effects on health of air pollution: a narrative review. *Intern. Emerg. Med.* **2015**, *10*, 657−662.

(15) Wyzga, R. E.; Rohr, A. C. Long-term particulate matter exposure: attributing health effects to individual PM components. *J. Air Waste Manage. Assoc.* **2015**, *65*, 523−543.

(16) Lelieveld, J.; Evans, J. S.; Fnais, M.; Giannadaki, D.; Pozzer, A. The contribution of outdoor air pollution sources to premature mortality on a global scale. *Nature* **2015**, *525*, 367−371.

(17) Phalen, R. F. *Inhalation Studies: Foundations and Techniques*; Informa Healthcare, 2009.

(18) Semeniuk, K.; Dastoor, A. Current state of atmospheric aerosol thermodynamics and mass transfer modeling: A review. *Atmosphere* **2020**, *11*, 156.

(19) Pankow, J. F. Review and comparative analysis of the theories on partitioning between the gas and aerosol particulate phases in the atmosphere. *Atmos. Environ.* **1987**, *21*, 2275−2283.

(20) Pankow, J. F. An absorption model of gas/particle partitioning of organic compounds in the atmosphere. *Atmos. Environ.* **1994**, *28*, 185−188.

(21) Pankow, J. F. An absorption model of the gas/aerosol partitioning involved in the formation of secondary organic aerosol. *Atmos. Environ.* **1994**, *28*, 189−193.

(22) Pankow, J. F. Further discussion of the octanol/air partition coefficient K_{OA} as a correlating parameter for gas/particle partitioning coefficients. *Atmos. Environ.* **1998**, *32*, 1493−1497.

(23) Donahue, N. M.; Ortega, I. K.; Chuang, W.; Riipinen, I.; Riccobono, F.; Schobesberger, S.; Dommen, J.; Baltensperger, U.; Kulmala, M.; Worsnop, D. R.; Vehkamaki, H. How do organic vapors contribute to new-particle formation? *Faraday Discuss.* **2013**, *165*, 91−104.

(24) Donahue, N. M.; Robinson, A. L.; Stanier, C. O.; Pandis, S. N. Coupled partitioning, dilution, and chemical aging of semivolatile organics. *Environ. Sci. Technol.* **2006**, *40*, 2635−2643.

(25) Shiraiwa, M.; Li, Y.; Tsimpidi, A. P.; Karydis, V. A.; Berkemeier, T.; Pandis, S. N.; Lelieveld, J.; Koop, T.; Pöschl, U. Global distribution of particle phase state in atmospheric secondary organic aerosols. *Nat. Commun.* **2017**, *8*, 15002.

(26) Zhou, S.; Shiraiwa, M.; McWhinney, R. D.; Pöschl, U.; Abbatt, J. P. D. Kinetic limitations in gas-particle reactions arising from slow

diffusion in secondary organic aerosol. *Faraday Discuss.* **2013**, *165*, 391−406.
(27) Kidd, C.; Perraud, V.; Wingen, L. M.; Finlayson-Pitts, B. J. Integrating phase and composition of secondary organic aerosol from the ozonolysis of α-pinene. *Proc. Natl. Acad. Sci. U.S.A.* **2014**, *111*, 7552−7557.
(28) Perraud, V.; Bruns, E. A.; Ezell, M. J.; Johnson, S. N.; Yu, Y.; Alexander, M. L.; Zelenyuk, A.; Imre, D.; Chang, W. L.; Dabdub, D.; Pankow, J. F.; Finlayson-Pitts, B. J. Nonequilibrium atmospheric secondary organic aerosol formation and growth. *Proc. Natl. Acad. Sci. U.S.A.* **2012**, *109*, 2836−2841.
(29) Shiraiwa, M.; Ammann, M.; Koop, T.; Pöschl, U. Gas uptake and chemical aging of semisolid organic aerosol particles. *Proc. Natl. Acad. Sci. U.S.A.* **2011**, *108*, 11003−11008.
(30) Pfrang, C.; Shiraiwa, M.; Pöschl, U. Chemical ageing and transformation of diffusivity in semi-solid multi-component organic aerosol particles. *Atmos. Chem. Phys.* **2011**, *11*, 7343−7354.
(31) Renbaum-Wolff, L.; Grayson, J. W.; Bateman, A. P.; Kuwata, M.; Sellier, M.; Murray, B. J.; Shilling, J. E.; Martin, S. T.; Bertram, A. K. Viscosity of α-pinene secondary organic material and implications for particle growth and reactivity. *Proc. Natl. Acad. Sci. U.S.A.* **2013**, *110*, 8014−8019.
(32) Vaden, T. D.; Imre, D.; Beránek, J.; Shrivastava, M.; Zelenyuk, A. Evaporation kinetics and phase of laboratory and ambient secondary organic aerosol. *Proc. Natl. Acad. Sci. U.S.A.* **2011**, *108*, 2190−2195.
(33) Abramson, E.; Imre, D.; Beránek, J.; Wilson, J.; Zelenyuk, A. Experimental determination of chemical diffusion within secondary organic aerosol particles. *Phys. Chem. Chem. Phys.* **2013**, *15*, 2983−2991.
(34) Bateman, A. P.; Bertram, A. K.; Martin, S. T. Hygroscopic influence on the semisolid-to-liquid transition of secondary organic materials. *J. Phys. Chem. A* **2015**, *119*, 4386−4395.
(35) Saukko, E.; Lambe, A. T.; Massoli, P.; Koop, T.; Wright, J. P.; Croasdale, D. R.; Pedernera, D. A.; Onasch, T. B.; Laaksonen, A.; Davidovits, P.; Worsnop, D. R.; Virtanen, A. Humidity-dependent phase state of SOA particles from biogenic and anthropogenic precursors. *Atmos. Chem. Phys.* **2012**, *12*, 7517−7529.
(36) Kuwata, M.; Martin, S. T. Phase of atmospheric secondary organic material affects its reactivity. *Proc. Natl. Acad. Sci. U.S.A.* **2012**, *109*, 17354−17359.
(37) Bell, D. M.; Imre, D.; Martin, S. T.; Zelenyuk, A. The properties and behavior of α-pinene secondary organic aerosol particles exposed to ammonia under dry conditions. *Phys. Chem. Chem. Phys.* **2017**, *19*, 6497−6507.
(38) Yli-Juuti, T.; Pajunoja, A.; Tikkanen, O.-P.; Buchholz, A.; Faiola, C.; Väisänen, O.; Hao, L.; Kari, E.; Peräkylä, O.; Garmash, O.; Shiraiwa, M.; Ehn, M.; Lehtinen, K.; Virtanen, A. Factors controlling the evaporation of secondary organic aerosol from α-pinene ozonolysis. *Geophys. Res. Lett.* **2017**, *44*, 2562−2570.
(39) Virtanen, A.; Joutsensaari, J.; Koop, T.; Kannosto, J.; Yli-Pirilä, P.; Leskinen, J.; Mäkelä, J. M.; Holopainen, J. K.; Pöschl, U.; Kulmala, M.; Worsnop, D. R.; Laaksonen, A. An amorphous solid state of biogenic secondary organic aerosol particles. *Nature* **2010**, *467*, 824−827.
(40) Li, Y. J.; Liu, P.; Gong, Z.; Wang, Y.; Bateman, A. P.; Bergoend, C.; Bertram, A. K.; Martin, S. T. Chemical reactivity and liquid/nonliquid states of secondary organic material. *Environ. Sci. Technol.* **2015**, *49*, 13264−13274.
(41) Zhao, Y.; Wingen, L. M.; Perraud, V.; Finlayson-Pitts, B. J. Phase, composition, and growth mechanism for secondary organic aerosol from the ozonolysis of α-cedrene. *Atmos. Chem. Phys.* **2016**, *16*, 3245−3264.
(42) Reid, J. P.; Bertram, A. K.; Topping, D. O.; Laskin, A.; Martin, S. T.; Petters, M. D.; Pope, F. D.; Rovelli, G. The viscosity of atmospherically relevant organic particles. *Nat. Commun.* **2018**, *9*, 956−969.
(43) Shiraiwa, M.; Seinfeld, J. H. Equilibration timescale of atmospheric secondary organic aerosol partitioning. *Geophys. Res. Lett.* **2012**, *39*, L24801.
(44) Charan, S. M.; Huang, Y.; Seinfeld, J. H. Computational simulation of secondary organic aerosol formation in laboratory chambers. *Chem. Rev.* **2019**, *119*, 11912−11944.
(45) Koop, T.; Bookhold, J.; Shiraiwa, M.; Pöschl, U. Glass transition and phase state of organic compounds: dependency on molecular properties and implications for secondary organic aerosols in the atmosphere. *Phys. Chem. Chem. Phys.* **2011**, *13*, 19238−19255.
(46) Vander Wall, A. C.; Lakey, P. S. J.; Rossich Molina, E.; Perraud, V.; Wingen, L. M.; Xu, J.; Soulsby, D.; Gerber, R. B.; Shiraiwa, M.; Finlayson-Pitts, B. J. Understanding interactions of organic nitrates with the surface and bulk of organic films: implications for particle growth in the atmosphere. *Environ. Sci.: Processes Impacts* **2018**, *20*, 1593−1610.
(47) Vander Wall, A. C.; Perraud, V.; Wingen, L. M.; Finlayson-Pitts, B. J. Evidence for a kinetically controlled burying mechanism for growth of high viscosity secondary organic aerosol. *Environ. Sci.: Processes Impacts* **2020**, *22*, 66−83.
(48) Abbatt, J. P. D.; Lee, A. K. Y.; Thornton, J. A. Quantifying trace gas uptake to tropospheric aerosol: recent advances and remaining challenges. *Chem. Soc. Rev.* **2012**, *41*, 6555−6581.
(49) Berkemeier, T.; Huisman, A. J.; Ammann, M.; Shiraiwa, M.; Koop, T.; Pöschl, U. Kinetic regimes and limiting cases of gas uptake and heterogeneous reactions in atmospheric aerosols and clouds: a general classification scheme. *Atmos. Chem. Phys.* **2013**, *13*, 6663−6686.
(50) Shrivastava, M.; Cappa, C. D.; Fan, J.; Goldstein, A. H.; Guenther, A. B.; Jimenez, J. L.; Kuang, C.; Laskin, A.; Martin, S. T.; Ng, N. L.; Petäjä, T.; Pierce, J. R.; Rasch, P. J.; Roldin, P.; Seinfeld, J. H.; Shilling, J.; Smith, J. N.; Thornton, J. A.; Volkamer, R.; Wang, J.; Worsnop, D. R.; Zaveri, R. A.; Zelenyuk, A.; Zhang, Q. Recent advances in understanding secondary organic aerosol: implications for global climate forcing. *Rev. Geophys.* **2017**, *55*, 509−559.
(51) Denjean, C.; Formenti, P.; Picquet-Varrault, B.; Pangui, E.; Zapf, P.; Katrib, Y.; Giorio, C.; Tapparo, A.; Monod, A.; Temime-Roussel, B.; Decorse, P.; Mangeney, C.; Doussin, J. F. Relating hygroscopicity and optical properties to chemical composition and structure of secondary organic aerosol particles generated from the ozonolysis of α-pinene. *Atmos. Chem. Phys.* **2015**, *15*, 3339−3358.
(52) Boyd, C. M.; Nah, T.; Xu, L.; Berkemeier, T.; Ng, N. L. Secondary organic aerosol (SOA) from nitrate radical oxidation of monoterpenes: effects of temperature, dilution, and humidity on aerosol formation, mixing, and evaporation. *Environ. Sci. Technol.* **2017**, *51*, 7831−7841.
(53) Gong, Z.; Han, Y.; Liu, P.; Ye, J.; Keutsch, F. N.; McKinney, K. A.; Martin, S. T. Influence of particle physical state on the uptake of medium-sized organic molecules. *Environ. Sci. Technol.* **2018**, *52*, 8381−8389.
(54) Han, Y.; Gong, Z.; Ye, J.; Liu, P.; McKinney, K. A.; Martin, S. T. Quantifying the role of the relative humidity-dependent physical state of organic particulate matter in the uptake of semivolatile organic molecules. *Environ. Sci. Technol.* **2019**, *53*, 13209−13218.
(55) Zelenyuk, A.; Imre, D.; Beránek, J.; Abramson, E.; Wilson, J.; Shrivastava, M. Synergy between secondary organic aerosols and long-range transport of polycyclic aromatic hydrocarbons. *Environ. Sci. Technol.* **2012**, *46*, 12459−12466.
(56) Kidd, C.; Perraud, V.; Finlayson-Pitts, B. J. New insights into secondary organic aerosol from the ozonolysis of α-pinene from combined infrared spectroscopy and mass spectrometry measurements. *Phys. Chem. Chem. Phys.* **2014**, *16*, 22706−22716.
(57) Zelenyuk, A.; Imre, D. G.; Wilson, J.; Bell, D. M.; Suski, K. J.; Shrivastava, M.; Beránek, J.; Alexander, M. L.; Kramer, A. L.; Massey Simonich, S. L. The effect of gas-phase polycyclic aromatic hydrocarbons on the formation and properties of biogenic secondary organic aerosol particles. *Faraday Discuss.* **2017**, *200*, 143−164.
(58) Shilling, J. E.; Chen, Q.; King, S. M.; Rosenoern, T.; Kroll, J. H.; Worsnop, D. R.; DeCarlo, P. F.; Aiken, A. C.; Sueper, D.; Jimenez,

https://dx.doi.org/10.1021/acsearthspacechem.0c00163
ACS Earth Space Chem. 2020, 4, 1435−1447

J. L.; Martin, S. T. Loading-dependent elemental composition of α-pinene SOA particles. *Atmos. Chem. Phys.* **2009**, *9*, 771−782.
(59) Claflin, M. S.; Krechmer, J. E.; Hu, W.; Jimenez, J. L.; Ziemann, P. J. Functional group composition of secondary organic aerosol formed from ozonolysis of α-pinene under high VOC and autoxidation conditions. *ACS Earth Space Chem.* **2018**, *2*, 1196−1210.
(60) Molteni, U.; Simon, M.; Heinritzi, M.; Hoyle, C. R.; Bernhammer, A.-K.; Bianchi, F.; Breitenlechner, M.; Brilke, S.; Dias, A.; Duplissy, J.; Frege, C.; Gordon, H.; Heyn, C.; Jokinen, T.; Kürten, A.; Lehtipalo, K.; Makhmutov, V.; Petäjä, T.; Pieber, S. M.; Praplan, A. P.; Schobesberger, S.; Steiner, G.; Stozhkov, Y.; Tomé, A.; Tröstl, J.; Wagner, A. C.; Wagner, R.; Williamson, C.; Yan, C.; Baltensperger, U.; Curtius, J.; Donahue, N. M.; Hansel, A.; Kirkby, J.; Kulmala, M.; Worsnop, D. R.; Dommen, J. Formation of highly oxygenated organic molecules from α-pinene ozonolysis: chemical characteristics, mechanism, and kinetic model development. *ACS Earth Space Chem.* **2019**, *3*, 873−883.
(61) Jain, S.; Fischer, K. B.; Petrucci, G. A. The influence of absolute mass loading of secondary organic aerosols on their phase state. *Atmosphere* **2018**, *9*, 131.
(62) Kolesar, K. R.; Chen, C.; Johnson, D.; Cappa, C. D. The influences of mass loading and rapid dilution of secondary organic aerosol on particle volatility. *Atmos. Chem. Phys.* **2015**, *15*, 9327−9343.
(63) Jensen, L. N.; Canagaratna, M. R.; Kristensen, K.; Quéléver, L. L. J.; Rosati, B.; Teiwes, R.; Glasius, M.; Pedersen, H. B.; Ehn, M.; Bilde, M. Temperature and VOC concentration as controlling factors for chemical composition of alpha-pinene derived secondary organic aerosol. *Atmos. Chem. Phys. Discuss.* **2020**, *2020*, 1−21.
(64) Gao, Y.; Hall, W. A.; Johnston, M. V. Molecular composition of monoterpene secondary organic aerosol at low mass loading. *Environ. Sci. Technol.* **2010**, *44*, 7897−7902.
(65) Kourtchev, I.; Giorio, C.; Manninen, A.; Wilson, E.; Mahon, B.; Aalto, J.; Kajos, M.; Venables, D.; Ruuskanen, T.; Levula, J.; Loponen, M.; Connors, S.; Harris, N.; Zhao, D.; Kiendler-Scharr, A.; Mentel, T.; Rudich, Y.; Hallquist, M.; Doussin, J.-F.; Maenhaut, W.; Bäck, J.; Petäjä, T.; Wenger, J.; Kulmala, M.; Kalberer, M. Enhanced Volatile Organic Compounds emissions and organic aerosol mass increase the oligomer content of atmospheric aerosols. *Sci. Rep.* **2016**, *6*, 35038.
(66) Jenkin, M. E.; Saunders, S. M.; Pilling, M. J. The tropospheric degradation of volatile organic compounds: a protocol for mechanism development. *Atmos. Environ.* **1997**, *31*, 81−104.
(67) Saunders, S. M.; Jenkin, M. E.; Derwent, R. G.; Pilling, M. J. Protocol for the development of the Master Chemical Mechanism, MCM v3 (Part A): tropospheric degradation of non-aromatic volatile organic compounds. *Atmos. Chem. Phys.* **2003**, *3*, 161−180.
(68) Jenkin, M. E.; Young, J. C.; Rickard, A. R. The MCM v3.3.1 degradation scheme for isoprene. *Atmos. Chem. Phys.* **2015**, *15*, 11433−11459.
(69) Zhao, Y.; Thornton, J. A.; Pye, H. O. T. Quantitative constraints on autoxidation and dimer formation from direct probing of monoterpene-derived peroxy radical chemistry. *Proc. Natl. Acad. Sci. U.S.A.* **2018**, *115*, 12142−12147.
(70) Ezell, M. J.; Johnson, S. N.; Yu, Y.; Perraud, V.; Bruns, E. A.; Alexander, M. L.; Zelenyuk, A.; Dabdub, D.; Finlayson-Pitts, B. J. A new aerosol flow system for photochemical and thermal studies of tropospheric aerosols. *Aerosol Sci. Technol.* **2010**, *44*, 329−338.
(71) Cavdar, H.; Saracoglu, N. Synthesis of new β-hydroxy nitrate esters as potential glycomimetics or vasodilators. *Eur. J. Org. Chem.* **2008**, 4615−4621.
(72) Jayne, J. T.; Leard, D. C.; Zhang, X.; Davidovits, P.; Smith, K. A.; Kolb, C. E.; Worsnop, D. R. Development of an aerosol mass spectrometer for size and composition analysis of submicron particles. *Aerosol Sci. Technol.* **2000**, *33*, 49−70.
(73) DeCarlo, P. F.; Kimmel, J. R.; Trimborn, A.; Northway, M. J.; Jayne, J. T.; Aiken, A. C.; Gonin, M.; Fuhrer, K.; Horvath, T.; Docherty, K. S.; Worsnop, D. R.; Jimenez, J. L. Field-deployable, high-resolution, time-of-flight aerosol mass spectrometer. *Anal. Chem.* **2006**, *78*, 8281−8289.
(74) Canagaratna, M. R.; Jayne, J. T.; Jimenez, J. L.; Allan, J. D.; Alfarra, M. R.; Zhang, Q.; Onasch, T. B.; Drewnick, F.; Coe, H.; Middlebrook, A.; Delia, A.; Williams, L. R.; Trimborn, A. M.; Northway, M. J.; DeCarlo, P. F.; Kolb, C. E.; Davidovits, P.; Worsnop, D. R. Chemical and microphysical characterization of ambient aerosols with the aerodyne aerosol mass spectrometer. *Mass Spectrom. Rev.* **2007**, *26*, 185−222.
(75) Canagaratna, M. R.; Jimenez, J. L.; Kroll, J. H.; Chen, Q.; Kessler, S. H.; Massoli, P.; Hildebrandt Ruiz, L.; Fortner, E.; Williams, L. R.; Wilson, K. R.; Surratt, J. D.; Donahue, N. M.; Jayne, J. T.; Worsnop, D. R. Elemental ratio measurements of organic compounds using aerosol mass spectrometry: characterization, improved calibration, and implications. *Atmos. Chem. Phys.* **2015**, *15*, 253−272.
(76) Fraser, R. T. M.; Paul, N. C. The mass spectrometry of nitrate esters and related compounds. Part I. *J. Chem. Soc. B* **1968**, *6*, 659−663.
(77) Bruns, E. A.; Perraud, V.; Zelenyuk, A.; Ezell, M. J.; Johnson, S. N.; Yu, Y.; Imre, D.; Finlayson-Pitts, B. J.; Alexander, M. L. Comparison of FTIR and particle mass spectrometry for the measurement of particulate organic nitrates. *Environ. Sci. Technol.* **2010**, *44*, 1056−1061.
(78) Rollins, A. W.; Fry, J. L.; Hunter, J. F.; Kroll, J. H.; Worsnop, D. R.; Singaram, S. W.; Cohen, R. C. Elemental analysis of aerosol organic nitrates with electron ionization high-resolution mass spectrometry. *Atmos. Meas. Tech.* **2010**, *3*, 301−310.
(79) Farmer, D. K.; Matsunaga, A.; Docherty, K. S.; Surratt, J. D.; Seinfeld, J. H.; Ziemann, P. J.; Jimenez, J. L. Response of an aerosol mass spectrometer to organonitrates and organosulfates and implications for atmospheric chemistry. *Proc. Natl. Acad. Sci. U.S.A.* **2010**, *107*, 6670−6675.
(80) Fraser, R. T. M.; Paul, N. C. The mass spectrometry of nitrate esters and related compounds. Part II. *J. Chem. Soc. B* **1968**, *140*, 1407−1410.
(81) Zelenyuk, A.; Yang, J.; Song, C.; Zaveri, R. A.; Imre, D. A new real-time method for determining particles' sphericity and density: application to secondary organic aerosol formed by ozonolysis of α-pinene. *Environ. Sci. Technol.* **2008**, *42*, 8033−8038.
(82) Fry, J. L.; Kiendler-Scharr, A.; Rollins, A. W.; Brauers, T.; Brown, S. S.; Dorn, H.-P.; Dubé, W. P.; Fuchs, H.; Mensah, A.; Rohrer, F.; Tillmann, R.; Wahner, A.; Wooldridge, P. J.; Cohen, R. C. SOA from limonene: role of NO_3 in its generation and degradation. *Atmos. Chem. Phys.* **2011**, *11*, 3879−3894.
(83) Ianni, J. C. *Kintecus*, 2017. www.kintecus.com.
(84) Sommariva, R.; Cox, S.; Martin, C.; Borońska, K.; Young, J.; Jimack, P. K.; Pilling, M. J.; Matthaios, V. N.; Nelson, B. S.; Newland, M. J.; Panagi, M.; Bloss, W. J.; Monks, P. S.; Rickard, A. R. AtChem (version 1), an open-source box model for the Master Chemical Mechanism. *Geosci. Model Dev.* **2020**, *13*, 169−183.
(85) Zhang, X.; Mcvay, R. C.; Huang, D. D.; Dalleska, N. F.; Aumont, B.; Flagan, R. C.; Seinfeld, J. H. Formation and evolution of molecular products in α-pinene secondary organic aerosol. *Proc. Natl. Acad. Sci. U.S.A.* **2015**, *112*, 14168−14173.
(86) Winterhalter, R.; Van Dingenen, R.; Larsen, B. R.; Jensen, N. R.; Hjorth, J. LC-MS analysis of aerosol particles from the oxidation of α-pinene by ozone and OH-radicals. *Atmos. Chem. Phys. Discuss.* **2003**, *3*, 1−39.
(87) Witkowski, B.; Gierczak, T. Early stage composition of SOA produced by α-pinene/ozone reaction: α-Acyloxyhydroperoxy aldehydes and acidic dimers. *Atmos. Environ.* **2014**, *95*, 59−70.
(88) Berndt, T.; Richters, S.; Jokinen, T.; Hyttinen, N.; Kurtén, T.; Otkjær, R. V.; Kjaergaard, H. G.; Stratmann, F.; Herrmann, H.; Sipilä, M.; Kulmala, M.; Ehn, M. Hydroxyl radical-induced formation of highly oxidized organic compounds. *Nat. Commun.* **2016**, *7*, 13677−13684.
(89) Iinuma, Y.; Böge, O.; Miao, Y.; Sierau, B.; Gnauk, T.; Herrmann, H. Laboratory studies on secondary organic aerosol formation from terpenes. *Faraday Discuss.* **2005**, *130*, 279−294.
(90) Li, X.; Chee, S.; Hao, J.; Abbatt, J. P. D.; Jiang, J.; Smith, J. N. Relative humidity effect on the formation of highly oxidized molecules

and new particles during monoterpene oxidation. *Atmos. Chem. Phys.* **2019**, *19*, 1555−1570.
(91) Grayson, J. W.; Zhang, Y.; Mutzel, A.; Renbaum-Wolff, L.; Böge, O.; Kamal, S.; Herrmann, H.; Martin, S. T.; Bertram, A. K. Effect of varying experimental conditions on the viscosity of α-pinene derived secondary organic material. *Atmos. Chem. Phys.* **2016**, *16*, 6027−6040.
(92) Aiken, A. C.; DeCarlo, P. F.; Jimenez, J. L. Elemental analysis of organic species with electron ionization high-resolution mass spectrometry. *Anal. Chem.* **2007**, *79*, 8350−8358.
(93) Duplissy, J.; DeCarlo, P. F.; Dommen, J.; Alfarra, M. R.; Metzger, A.; Barmpadimos, I.; Prevot, A. S. H.; Weingartner, E.; Tritscher, T.; Gysel, M.; Aiken, A. C.; Jimenez, J. L.; Canagaratna, M. R.; Worsnop, D. R.; Collins, D. R.; Tomlinson, J.; Baltensperger, U. Relating hygroscopicity and composition of organic aerosol particulate matter. *Atmos. Chem. Phys.* **2011**, *11*, 1155−1165.
(94) Ng, N. L.; Canagaratna, M. R.; Zhang, Q.; Jimenez, J. L.; Tian, J.; Ulbrich, I. M.; Kroll, J. H.; Docherty, K. S.; Chhabra, P. S.; Bahreini, R.; Murphy, S. M.; Seinfeld, J. H.; Hildebrandt, L.; Donahue, N. M.; DeCarlo, P. F.; Lanz, V. A.; Prévôt, A. S. H.; Dinar, E.; Rudich, Y.; Worsnop, D. R. Organic aerosol components observed in Northern Hemispheric datasets from aerosol mass spectrometry. *Atmos. Chem. Phys.* **2010**, *10*, 4625−4641.
(95) Jimenez, J. L.; Canagaratna, M. R.; Donahue, N. M.; Prevot, A. S. H.; Zhang, Q.; Kroll, J. H.; DeCarlo, P. F.; Allan, J. D.; Coe, H.; Ng, N. L.; Aiken, A. C.; Docherty, K. S.; Ulbrich, I. M.; Grieshop, A. P.; Robinson, A. L.; Duplissy, J.; Smith, J. D.; Wilson, K. R.; Lanz, V. A.; Hueglin, C.; Sun, Y. L.; Tian, J.; Laaksonen, A.; Raatikainen, T.; Rautiainen, J.; Vaattovaara, P.; Ehn, M.; Kulmala, M.; Tomlinson, J. M.; Collins, D. R.; Cubison, M. J.; Dunlea, J.; Huffman, J. A.; Onasch, T. B.; Alfarra, M. R.; Williams, P. I.; Bower, K.; Kondo, Y.; Schneider, J.; Drewnick, F.; Borrmann, S.; Weimer, S.; Demerjian, K.; Salcedo, D.; Cottrell, L.; Griffin, R.; Takami, A.; Miyoshi, T.; Hatakeyama, S.; Shimono, A.; Sun, J. Y.; Zhang, Y. M.; Dzepina, K.; Kimmel, J. R.; Sueper, D.; Jayne, J. T.; Herndon, S. C.; Trimborn, A. M.; Williams, L. R.; Wood, E. C.; Middlebrook, A. M.; Kolb, C. E.; Baltensperger, U.; Worsnop, D. R. Evolution of organic aerosols in the atmosphere. *Science* **2009**, *326*, 1525−1529.
(96) Turpin, B. J.; Huntzicker, J. J. Identification of secondary organic aerosol episodes and quantitation of primary and secondary organic aerosol concentrations during SCAQS. *Atmos. Environ.* **1995**, *29*, 3527−3544.
(97) de Gouw, J. A.; Middlebrook, A. M.; Warneke, C.; Goldan, P. D.; Kuster, W. C.; Roberts, J. M.; Fehsenfeld, F. C.; Worsnop, D. R.; Canagaratna, M. R.; Pszenny, A. A. P.; Keene, W. C.; Marchewka, M.; Bertman, S. B.; Bates, T. S. Budget of organic carbon in a polluted atmosphere: Results from the New England Air Quality Study in 2002. *J. Geophys. Res.: Atmos.* **2005**, *110*, D16305.
(98) Zhang, Q.; Jimenez, J. L.; Canagaratna, M. R.; Allan, J. D.; Coe, H.; Ulbrich, I.; Alfarra, M. R.; Takami, A.; Middlebrook, A. M.; Sun, Y. L.; Dzepina, K.; Dunlea, E.; Docherty, K.; DeCarlo, P. F.; Salcedo, D.; Onasch, T.; Jayne, J. T.; Miyoshi, T.; Shimono, A.; Hatakeyama, S.; Takegawa, N.; Kondo, Y.; Schneider, J.; Drewnick, F.; Borrmann, S.; Weimer, S.; Demerjian, K.; Williams, P.; Bower, K.; Bahreini, R.; Cottrell, L.; Griffin, R. J.; Rautiainen, J.; Sun, J. Y.; Zhang, Y. M.; Worsnop, D. R. Ubiquity and dominance of oxygenated species in organic aerosols in anthropogenically-influenced Northern Hemisphere midlatitudes. *Geophys. Res. Lett.* **2007**, *34*, L13801.
(99) Riipinen, I.; Pierce, J. R.; Yli-Juuti, T.; Nieminen, T.; Häkkinen, S.; Ehn, M.; Junninen, H.; Lehtipalo, K.; Petäjä, T.; Slowik, J.; Chang, R.; Shantz, N. C.; Abbatt, J.; Leaitch, W. R.; Kerminen, V.-M.; Worsnop, D. R.; Pandis, S. N.; Donahue, N. M.; Kulmala, M. Organic condensation: a vital link connecting aerosol formation to cloud condensation nuclei (CCN) concentrations. *Atmos. Chem. Phys.* **2011**, *11*, 3865−3878.
(100) Slade, J. H.; Ault, A. P.; Bui, A. T.; Ditto, J. C.; Lei, Z.; Bondy, A. L.; Olson, N. E.; Cook, R. D.; Desrochers, S. J.; Harvey, R. M.; Erickson, M. H.; Wallace, H. W.; Alvarez, S. L.; Flynn, J. H.; Boor, B. E.; Petrucci, G. A.; Gentner, D. R.; Griffin, R. J.; Shepson, P. B. Bouncier particles at night: Biogenic secondary organic aerosol chemistry and sulfate drive diel variations in the aerosol phase in a mixed forest. *Environ. Sci. Technol.* **2019**, *53*, 4977−4987.
(101) Pajunoja, A.; Hu, W.; Leong, Y. J.; Taylor, N. F.; Miettinen, P.; Palm, B. B.; Mikkonen, S.; Collins, D. R.; Jimenez, J. L.; Virtanen, A. Phase state of ambient aerosol linked with water uptake and chemical aging in the southeastern US. *Atmos. Chem. Phys.* **2016**, *16*, 11163−11176.
(102) Moller, B.; Rarey, J.; Ramjugernath, D. Estimation of the vapour pressure of non-electrolyte organic compounds via group contributions and group interactions. *J. Mol. Liq.* **2008**, *143*, 52−63.
(103) Nannoolal, Y.; Rarey, J.; Ramjugernath, D.; Cordes, W. Estimation of pure component properties: Part 1. Estimation of the normal boiling point of non-electrolyte organic compounds via group contributions and group interactions. *Fluid Phase Equilib.* **2004**, *226*, 45−63.
(104) Pankow, J. F.; Asher, W. E. SIMPOL.1: a simple group contribution method for predicting vapor pressures and enthalpies of vaporization of multifunctional organic compounds. *Atmos. Chem. Phys.* **2008**, *8*, 2773−2796.
(105) Vander Wall, A.; Wingen, L. M.; Perraud, V.; Zhao, Y.; Finlayson-Pitts, B. J. Supplementary data for enhanced gas uptake during α-pinene ozonolysis points to a burying mechanism. *UC Irvine DRYAD*, Dataset, https://doi.org/10.7280/D1M67M.

https://dx.doi.org/10.1021/acsearthspacechem.0c00163
ACS Earth Space Chem. 2020, 4, 1435−1447